Available online at www.sciencedirect.com

SciVerse ScienceDirect

Ceramics International 38 (2012) 6365–6375

CERAMICS INTERNATIONAL

www.elsevier.com/locate/ceramint

Effect of annealing on the phase transition and morphology of Ag NPs on/in TiO_2 rods synthesized by a polyol method

Altangerel Amarjargal[a,b], Leonard D. Tijing[c,*], Cheol Sang Kim[a,c,*]

[a]Department of Bionanosystem Engineering, Chonbuk National University, Jeonju, Jeonbuk 561-756, Republic of Korea
[b]Power Engineering School, Mongolian University of Science and Technology, Ulaanbaatar, Mongolia
[c]Division of Mechanical Design Engineering, Chonbuk National University, Jeonju, Jeonbuk 561-756, Republic of Korea

Received 29 March 2012; received in revised form 24 April 2012; accepted 4 May 2012
Available online 14 May 2012

Abstract

In this study, we report the effect of annealing (250–700 °C) on the phase transition and morphology of silver (Ag) nanoparticles (NPs) on/in titanium dioxide (TiO_2) rods prepared using a polyol method. The annealed samples showed not only morphological change, i.e., a solid-to-liquid (melting) transition of Ag NPs due to its partial dissolution into the TiO_2 rods, but also early stage anatase crystallization and anatase–rutile transformation of TiO_2 rods under low annealing temperatures. Such findings, together with XRD and FE-SEM analyses, confirm that, upon higher annealing treatment, diffusion and coalescence leads to changes in the size and shape of the metal particles not only in the outermost regions, but also a random distribution and progressive growth of Ag clusters in the inner interface region. Here, it was shown that annealing can induce changes in morphology, as well as the chemical state and structure of Ag–TiO_2. The present polyol-synthesized Ag–TiO_2 composite also showed improved thermal stability.

Keywords: A. Calcination; B. Nanocomposites; D. TiO_2; Phase transition

1. Introduction

In recent years, the development of nanocomposite materials with metal particles in/on various organic and inorganic host matrices has been widely investigated in materials sciences due to their enhanced properties and potential application in optics, energy storage, catalysis, sensors, drug delivery, cancer therapy and environmental remediation [1–10]. Silver (Ag) nanoparticles (NPs) supported on one-dimensional (1D) TiO_2 nanostructures such as nanorods, nanowires, nanotubes, nanobelts, and nanofibers have attracted much attention not only because TiO_2 is a promising substrate material with desirable electronic and optical properties, but also because Ag displays some unique activities in chemical and biological sensing compared with other noble metals [11]. Nam et al. [12] synthesized Ag@1D-TiO_2 nanofibers using a simple one-step electrospinning method, and suggested that the controlled incorporation of metallic nanoparticles into a 1D Li host matrix may be a promising approach for realizing high-rate Li-ion storage devices. Liang et al. [13] reported the excellent performance of Ag nanoparticles deposited on TiO_2 nanotube catalysts, which can be attributed to the following three aspects. First, the well-dispersed Ag nanoparticles on the surface of TiO_2 nanotubes (Ag simultaneously doped and deposited on TiO_2 nanotubes) result in a higher electrochemical surface area and much better electrocatalytic activity. Second, Ag works as the main dehydrogenation site, and the more exposed Ag (1 1 1) surface on Ag NPs can lead to higher activity. Third, the anatase TiO_2 facilitates the removal of the CO-containing intermediates, leading to an enhanced catalytic activity.

The physical and chemical properties, and phase transition of substrate-supported metal NPs themselves are usually temperature and substrate dependent, respectively. It is therefore important to investigate the effect of the substrates on the phase transition of these NPs due to its

*Corresponding authors. Fax: +82 63 270 2460.
E-mail addresses: ltijing@jbnu.ac.kr (L.D. Tijing), chskim@jbnu.ac.kr (C.S. Kim).

0272-8842/$36.00 © 2012 Elsevier Ltd and Techna Group S.r.l. All rights reserved.
http://dx.doi.org/10.1016/j.ceramint.2012.05.009

close proximity with the solid contact. It is necessary to directly confirm whether a nanometer-sized particle on a substrate would undergo a solid-to-gas transition prior to the disappearance of the whole particle or whether a particle would first undergo a solid-to-liquid (i.e., melting) transition and then undergo a liquid-to-gas transition until all the constituent atoms of the particle evaporate. It is also of interest to examine the change in morphology of a particle during such a solid-to-gas (or liquid-to-gas) transition as a function of particle size [14–17]. In a previous work [18] by our group, TiO_2 microrods in situ decorated with Ag nanoparticles were successfully synthesized via a one pot method. We found that the annealing temperature influences the size of Ag NPs, which could influence its antibacterial effects.

However, to our best knowledge, an investigation of the effect of annealing treatment on the phase transition and morphology of supported Ag NPs and TiO_2 host matrix has not yet been performed. The present study describes how increasing annealing temperature affects the phase transition and morphology change of two different materials, i.e., Ag NPs and TiO_2 microrods, and how the resulting early stage anatase crystallization, and promoted anatase to rutile transformation of TiO_2 rods cause the deposition of metallic silver (Ag^0) nanoparticles.

2. Experimental

2.1. Sample preparation

The following chemicals were used as purchased without further purification: titanium (IV) isopropoxide (TIPP, guaranteed reagent, Junsei), silver nitrate ($AgNO_3$, Showa), poly(vinylpyrrolidone) (PVP, Alfa Aesar, MW=58,000), and ethylene glycol (EG, Showa). Ag NPs and nanoporous TiO_2 rods were simultaneously synthesized using a reflux method followed by heat treatment. An experimental procedure similar to that described by Xia et al. [19,20] was used in this study with modifications, as described in our previous report [18]. Briefly, ethylene glycol was employed as the reduction medium as well as the solvent, silver nitrate ($AgNO_3$) and titanium (IV) isopropoxide as precursors, and PVP as a polymer capping reagent. First, 100 ml EG and 1 ml TIPP were refluxed under vigorous stirring at 170 °C for 90 min. Then, 10 mL EG (dissolved in 0.33 g PVP) was added to the hot solution. Soon after, different amounts of aqueous $AgNO_3$ ($1.6\times10^{-2}$and 8×10^{-3} M) were introduced into the mixture solution that had already produced titanium glycolate rods, and from this point, the reaction was maintained at 150 °C for 30 min. Finally, the solution was cooled to room temperature and the synthesized rods were separated by vacuum filtration. Dark gray precipitate was subsequently washed by de-ionized (DI) water and ethanol, and then dried to room temperature for one day. Finally, the as-prepared sample was annealed at 250 °C, 350 °C, 500 °C and 700 °C for 2 h at a heating rate of 5 °C/min in air using an electric furnace (SH-MFIC, Samheung, Korea). In addition, pure nanoporous TiO_2 rods were also prepared using the same method but without a $AgNO_3$ precursor.

2.2. Characterization

X-ray powder diffraction (XRD) analysis was carried out using a Rigaku X-ray diffractometer (Cu Kα, $\lambda=1.54059$ Å) over Bragg angles ranging from 20° to 80°. Surface states of the samples were surveyed by X-ray photoelectron spectroscopy (XPS, AXIS-NOVA, Kratos, Inc.) with an Al Kα irradiation source. All binding energy values were determined by calibration and fixing the C(1s) core level line to 284.6 eV. The surface structures and morphologies of the samples were studied by field emission scanning electron microscopy (FE-SEM, S-7400, Hitachi, Japan), and an energy dispersive spectrometer (EDS) was used to check the elemental composition. The particle size and distribution were determined using a transmission electron microscope (TEM, JEOL JEM, Japan) at an accelerating voltage of 200 kV. FTIR spectra of the samples were obtained using a Paragon 1000 Spectrometer (Perkin Elmer). The signal resolution of the FTIR was 1 cm^{-1} and a minimum of 16 scans were obtained and averaged within the range of 400–4000 cm^{-1}. Thermogravimetric analysis (TGA) was performed in a nitrogen atmosphere at a rate of 10 °C/min using a TGA Q50 (TA Instruments, USA).

3. Results and discussion

3.1. XRD

XRD spectra of the as-synthesized and annealed samples of Ag NP-impregnated TiO_2 rods with different amounts of $AgNO_3$ at various temperatures are shown in Fig. 1. All the Ag–TiO_2 composites represented metallic silver NPs, which possessed good crystallinity and high purity with 4 peaks in the range of $2\theta=37.75$–77.2°, assigned as (1 1 1), (2 0 0), (2 2 0) and (3 1 1) planes. In the as-synthesized sample, only these Ag peaks are seen with high intensity, which leads to the conclusion that the silver is well-dispersed on the surface of the titanium glycolate host matrix. Compared with Ag peaks of the as-synthesized sample (Fig. 1a), the decrease and broadening of the Ag peaks under a low annealing temperature (i.e., at 250 and 350 °C) (Fig. 1b and c) may be due to the partial dissolution of silver into the host matrix, and the occurrence of Ag^0 to Ag^+ oxidation. Armela et al. [21] observed that an appreciable decrease in both the Auger parameters to values intermediate between those of Ag° and Ag^+ upon annealing at 400 °C in air, thus suggesting an appreciable Ag°–Ag^+ oxidation under their given conditions. As the annealing temperatures were increased to 500 and 700 °C (Fig. 1d and e), the XRD peaks, assigned to the metallic Ag structure, became stronger and sharper, when compared to the as-synthesized and for lower temperature-annealed samples. This observation

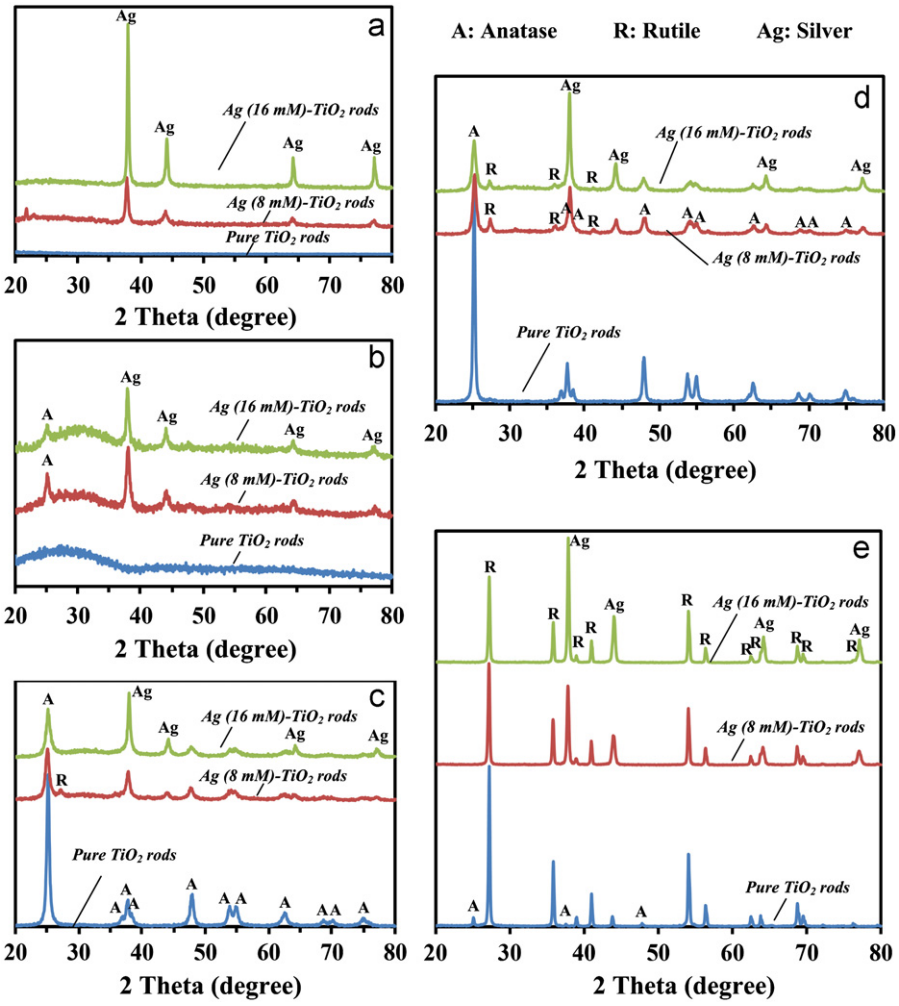

Fig. 1. XRD spectra of the (a) as-synthesized TiO_2 sample, annealed pure TiO_2 and Ag–TiO_2 samples at (b) 250 °C, (c) 350 °C, (d) 500 °C, and (e) 700 °C.

suggests that Ag^+ ions are then reduced to Ag° with heat due to the high redox potential of Ag^+, the low stability of the Ag^+ complex in TiO_2, and the greater electron donation ability of TiO_2 [22]. The initiation of Ag ion reduction demands strong reductive agents as the Ag^+/Ag° potential is relatively high [23], and electron liberation from titania facilitates the reduction process [24]. In addition, because Ag–O bonding is much weaker than Ti–O and Ag–Ag bonding, and Ag atoms possess higher surface free energy than TiO_2, newly formed Ag clusters have the tendency to aggregate into larger Ag particles during annealing at higher temperatures [25–27].

In the as-synthesized sample (Fig. 1a), there was no sign of any TiO_2 crystal structure, which means that the Ag/TiO_2 microrods are predominantly amorphous. However, various diffraction lines of TiO_2, corresponding to anatase and rutile phases, can be clearly seen for all composite samples (Fig. 1b–e), indicating that the annealed samples were well-crystallized after the heat treatment. In particular, a relatively weak diffraction peak at $2\theta = 25.1°$, corresponding to the anatase crystallization starts to appear in the XRD patterns of annealed Ag–TiO_2 samples (Fig. 1b) [28]. The increase in the intensity of characteristic anatase peaks becomes more significant for both pure and Ag NP impregnated TiO_2 rods at an annealing temperature of 350 °C (Fig. 1c). Interestingly, we observed early stage anatase crystallization and anatase to rutile transformation corresponding to annealing at 250 °C and 350 °C, respectively, i.e., at lower annealing temperatures, which is in accordance with the observation of Akgun et al. who observed more defined early stage anatase crystallization when they subjected their thin film with high Ag concentration to heat treatment at 250 °C [29]. In the present study, upon annealing at 500 °C (Fig. 1d), more well-defined diffraction peaks of the rutile phase emerge for Ag–TiO_2 microrods with different amounts of $AgNO_3$, while the pure sample did not show any rutile peaks, indicating that the Ag^+ ion and NPs can promote phase transition from anatase to rutile.

Table 1 shows the average anatase grain size of the pure and Ag NPs impregnated TiO_2 microrods, as determined by calculation from the broadening of the anatase (1 0 1) peak ($\theta = 25.15°$) using the Scherrer equation (Eq. 1):

$$d = \frac{(K\lambda)}{(B\cos\theta)}, \quad (1)$$

Table 1
Effects of annealing temperature on the mean size of Ag NPs and the average anatase grain size (nm).

	Annealing temperature									
	As-synthesized		250 °C		350 °C		500 °C		700 °C	
	Ag	TiO_2	Ag	TiO_2	Ag	TiO_2	Ag	TiO_2	Ag	TiO_2
PureTiO_2	–	–	–	–	–	17	–	24	–	35[a]
Ag(8 mM)–TiO_2(nm)	14	–	11	6	12	11	19	16	28	62[a]
Ag(16 mM)–TiO_2(nm)	33	–	13	4	19	10	28	14	42	65[a]

[a]Average rutile grain size, which was determined from the intensity of the rutile (1 1 0) peak.

where d is the average rutile grain size; $K=0.89$ is the Scherrer constant; λ is the wavelength of the X-ray (for Cu Ka, $\lambda=1.54056$A°,); θ is the diffraction angle; and B is the full width at half maximum (in radians). The enhancement in the TiO_2 phase transition is accelerated after thermal reduction of Ag^+ to Ag°due to the following several factors [29–31]. One is that, the increase in annealing temperature resulted in a decrease of the anatase grain sizes of the Ag–TiO_2 composites with respect to the pure TiO_2 sample (see Table 1), which increases the total boundary energy for TiO_2 powder. The driving force for rutile grain growth then increases and the anatase to rutile phase transformation is promoted [32]. Moreover, phase transition is also governed by such effects as defect concentration and grain boundary concentration, the presence of which can be expected to be increased with greater surface area. Chao et al. [30] reported that with the specific surface area increasing, the density of surface defects at the surface of anatase grains, which are considered to be the rutile nucleation sites for TiO_2 powders with relatively high specific surface areas, would increase. Rutile nucleation is thus enhanced as the presence of defect sites is increased. Therefore, an increase in the density of surface defects promotes anatase to rutile transformation at lower temperatures. Defects on the TiO_2 (1 1 0) surface are easily created by electron bombardment, sputtering, or simply by thermal annealing the surface to high temperatures. Thermally-created defects have been recognized extensively in the literature as point defects that exist as oxygen vacancy sites located within the bridging oxygen rows of the TiO_2 surface [33]. Another factor is that the concentration of oxygen vacancies at the surface of anatase grains increases in the presence of Ag ion or Ag particles, which favors ionic rearrangement and structure reorganization for the rutile phase [30]. In order to further demonstrate the promotion of phase transition, the annealing temperature was increased up to 700 °C. From the diffraction patterns (Fig. 1e), there were only the rutile peaks, and there was an absence of any peak characteristic of the anatase phase in the composite samples. However, in the case of TiO_2 microrods, a considerable amount of the anatase remains in the powder. Because the radius of the Ag^+ ion (ca 126 pm) is much larger that the Ti^{4+} ion (ca 68 pm), Ag^+ ions cannot enter the anatase lattice to form a stable solid solution. During the calcination process, with the elimination of liquids and organic substances and the crystallization of the anatase phase, the uniformly-dispersed Ag ions will gradually migrate from the volume of the anatase grains to the surface, and further to the surface of the TiO_2 powder under the action of heat [30]. The energy necessary for movement of the anatase grain boundary then increases, and the driving force for the anatase grain boundary migration decreases [34]. Anatase grain growth is thereby depressed.

In the literature, studies of the effect of annealing treatment on the phase transition of Ag–TiO_2 composites do not show consistent results. In some cases, it was reported that Ag particles partially inhibit or do not affect crystallization [35–37]. Okumu et al. [36] observed that delayed crystallization occurred in the presence of silver atoms due to the fine dispersion of silver NPs in the amorphous TiO_2 matrix by sputtering a thin silver film sandwiched between TiO_2 layers. Interestingly, the above-mentioned study used a protected annealing atmosphere, i.e., argon and vacuum. Yet, in the present case, the early stage anatase crystallization and promotion of anatase to rutile transformation may not only be caused by impregnated silver NPs on the surfaces of titanium glycolate microrods, but also may be because the composite sample was annealed in an air atmosphere. Similar phenomena have also been reported for Ag/TiO_2 nanosystems prepared by the radio-frequency sputtering of silver particles on titania based xerogels prepared by the sol–gel route [21]. Therefore, it could be deduced that the thermal stability of the anatase phase depends strongly on both the Ag doping and annealing conditions [38].

3.2. Morphological characterization

Ag NPs deposited on the TiO_2 microrods were produced by one pot synthesis followed by post-annealing treatment. Only one synthesis medium (ethylene glycol) was used, leading to two different morphologies i.e., Ag NPs and TiO_2 microrods. The morphology of annealed TiO_2 and Ag–TiO_2 rods are shown in Fig. 2. FE-SEM images (Fig. 2) reveal the presence of numerous TiO_2 rods with lengths ranging from several micrometers to several tens of micrometers, and their diameters are about 0.5–5 μm. In previous studies, when titanium alkoxide was added to EG and heated to 170 °C for 2 h under rigorous stirring, the

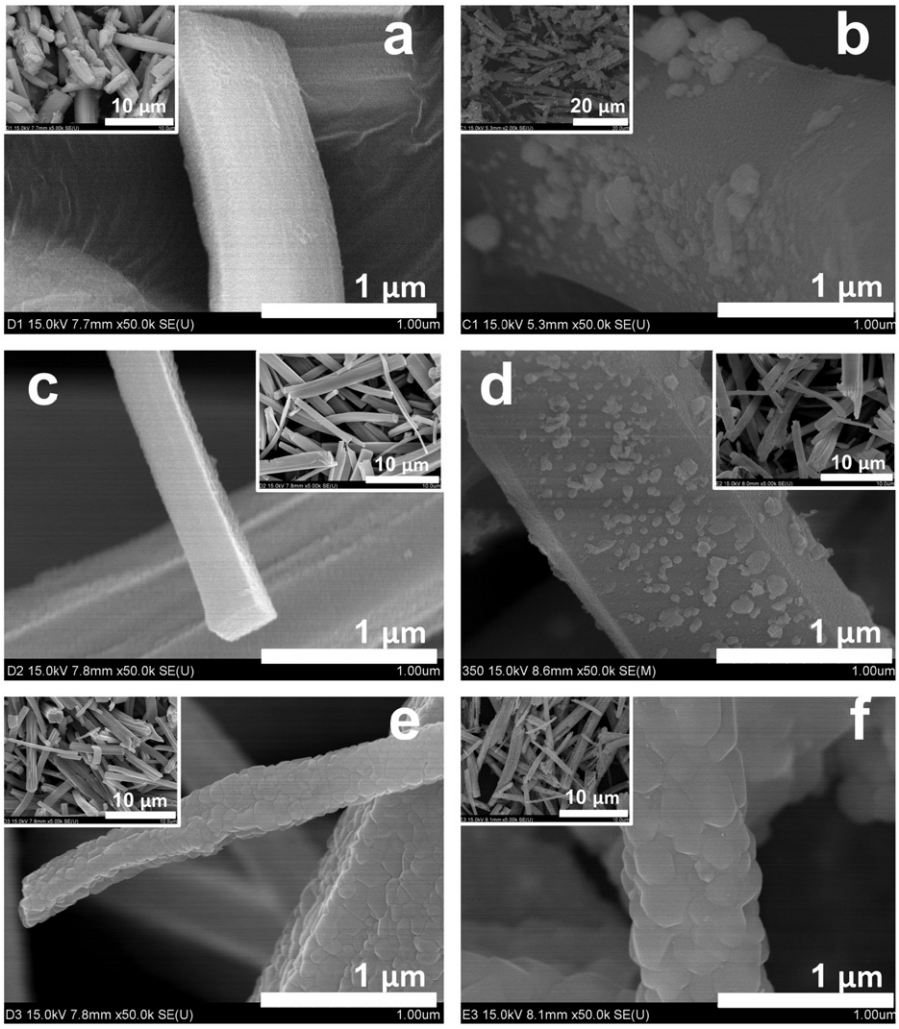

Fig. 2. FE-SEM images of as-synthesized samples of (a) pure TiO_2 and (b) Ag–TiO_2, and annealed samples at 500 °C (c,d) and 700 °C (e,f) of pure TiO_2 (c,e) and Ag–TiO_2 (d,f). The respective insets show their low magnification images. The results shown here are for a concentration of 16 mM $AgNO_3$.

alkoxide was transformed into a chain-like, glycolate complex that subsequently crystallized into uniform nanowires or nanorods, and that titanium glycolate converts into TiO_2 under high temperature annealing [20,39,40]. Based on the FE-SEM images (Fig. 2b, d and f), the one-pot method for the synthesis of NPs leads to the formation and random distribution of Ag NPs on the TiO_2 microrods. We used low molecular weight PVP as a capping agent to help lessen the Ag NP aggregation, but, some primary NPs coalesce with other primary NPs and formed bigger NPs. Because of the relatively high temperature used in the synthesis of silver particles, the Brownian motion and mobility of surface atoms increased. This enhances the probability of particle collision, adhesion, and subsequent coalescence [41]. These nanosized silver particles with broad size, which were pseudo-spherical and irregular in shape that attached to the surface of the TiO_2 microrods, can be observed more clearly in the image of an individual as-synthesized Ag–TiO_2 rod (Fig. 2d). Interestingly, we found that the annealing process induced some changes in the shape and size of Ag particles, probably due to the crystalline-to-liquid transition (i.e., melting) on the host matrix [14]. As Tang et al. [16] suggested, there are two main aspects for the process favorable to the shape evolution of Ag NPs, namely, surface diffusion, and premelting. Unlike surface diffusion, surface premelting of Ag NPs takes place beyond a certain temperature, and it induces the formation of a liquid layer covering the Ag solid.

TEM analyses (Fig. 3) give further and direct evidence of the nanoporous TiO_2 rods and the existence of Ag NPs on/in TiO_2 microrods with respect to various annealing treatments. The TEM images depict that the as-synthesized titanium glycolate rods (Fig. 3a) are composed of NPs in an aggregated to nanoporous geometry, which turn into rods consisting of numerous anatase and rutile TiO_2 NPs (Fig. 3c and e), corresponding to annealing at 500 °C (Fig. 3c) and 700 °C (Fig. 3e), respectively. The morphology of Ag–TiO_2 rods was found to be quite similar to TiO_2 rods (Fig. 3b). As shown in Fig. 3b, NPs of metallic silver with size varying from 40 nm to 60 nm, are anchored strongly on the surface of titanium glycolate rods. While the relatively smooth surfaces of the support complex

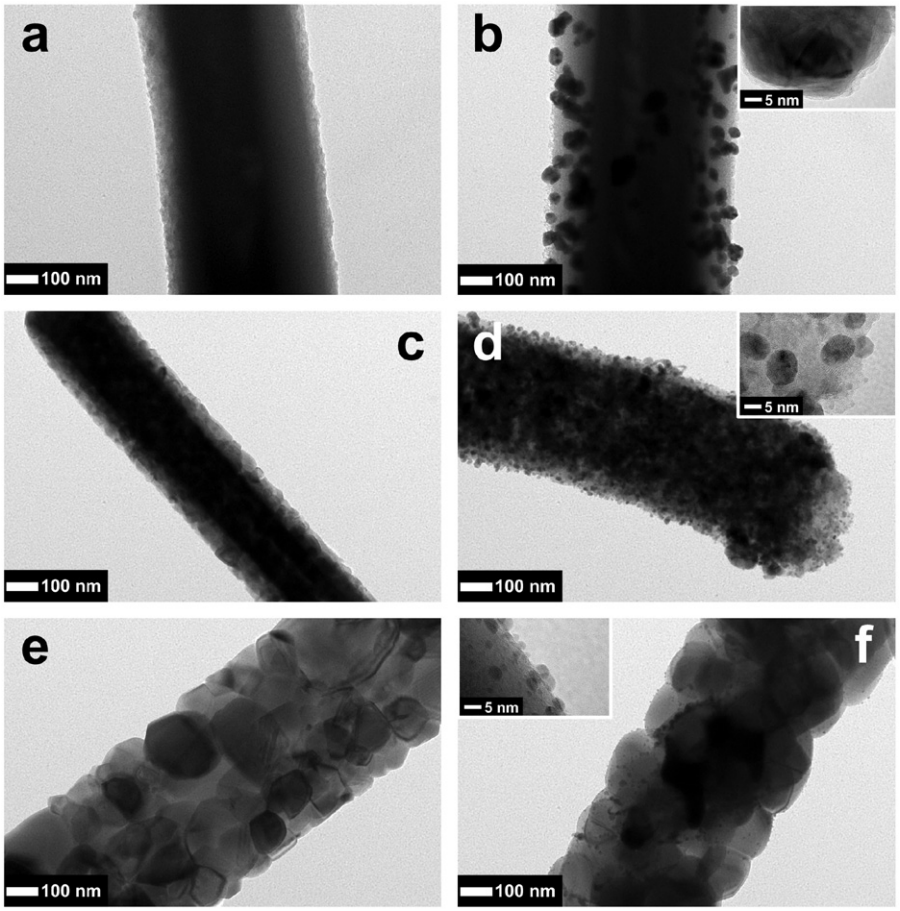

Fig. 3. TEM images of as-synthesized samples of (a) pure TiO_2 and (b) Ag–TiO_2, and annealed samples at 500 °C (c,d) and 700 °C (e,f) of pure TiO_2 (c,e) and Ag–TiO_2 (d,f). The respective insets show their low magnification images. The results shown here are for a concentration of 16 mM $AgNO_3$.

(titanium glycolate) were significantly roughened, the mean size of the supported Ag-containing aggregates was appreciably reduced after subsequent annealing treatment due to the partial silver dissolution discussed above. It is found that the amorphous structure of the host matrix allows silver to diffuse more easily, and therefore forms larger silver particles [42]. In particular, there are only a few Ag clusters on the TiO_2 surface for the annealed sample at 700 °C (Fig 3f), indicating that its morphological modifications were induced by the annealing process. Such findings, together with the evidence provided by X-ray diffraction and FE-SEM analyses, confirm that upon higher annealing treatment, diffusion and coalescence leads to changes in the size and shape of metal particles not only in the outermost regions, but also in the random distribution and progressive growth of Ag clusters in the inner interface region [21,37]. The phenomena of morphological modifications and phase transitions induced by thermal treatment for Ag NPs are dependent on their size and support matrix. In a systematic in situ TEM study by Asoro et al. [43], relating to the size effect on the melting temperature of individual Ag NPs, it was demonstrated that the NPs labeled A–K, in order of increasing size, either vanish from the support or shrink in size before eventually disappearing as the temperature increases. Chen et al. [14] also observed no crystalline-to-liquid transition, but only a crystalline-to-gas transition (i.e., sublimation) took place in the silver NPs on the graphite substrate prior to their complete disappearance; further, a crystalline-to-liquid transition did take place in the silver NPs on the alumina substrate. In addition, the Ag particle size distribution on the TiO_2 microrods was very narrow, and without any observable agglomeration for annealed samples. In this regard, it is important to note that the shape, size, and distribution of Ag NPs can be modified by thermal annealing.

We used high-resolution TEM (HRTEM) and nanodiffraction patterns to study the morphology and internal crystalline structures of the obtained composite samples. HRTEM images of TiO_2 and Ag single particles, located in different areas, are shown in Fig. 4a and b, where clear lattice fringes can be observed. The corresponding selected-area electron diffraction (SAED) patterns and Fourier spectra (equivalent to optical diffraction patterns), obtained by the fast Fourier transformation (FFT) process from the HRTEM images are also shown in their respective insets (Fig. 4a and b). The nanocrystals, with a lattice fringe of 0.35 (Fig. 4a) and 0.23 nm (Fig. 4b), are attributed to the

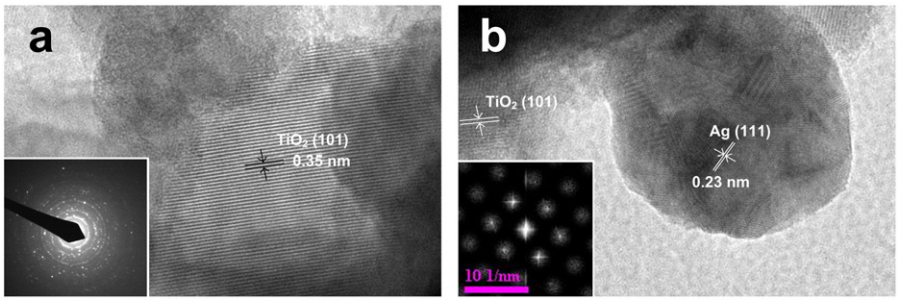

Fig. 4. HRTEM images of Ag–TiO_2 composite annealed at 500 °C (16 mM $AgNO_3$) at two different areas (a,b). The insets are the (a) SAED and (b) FFT images of the same sample.

spacing of (1 0 1) in anatase TiO_2 and (1 1 1) in Ag, respectively. The diffraction spots/rings, corresponding to various orientations of the nanocrystals, which appear inside the concentric rings (Fig. 4a inset), clearly showed that Ag–TiO_2 rods had good crystallinity, which agrees well with the results of the XRD analysis.

In the present synthesis, titanium glycolate was first produced by the heating of titanium alkoxide in an ethylene glycol medium, and then the hot ethylene glycol solution reduced the silver nitrate, followed by the nucleation of metallic silver and growth of silver NPs. In other words, titanium glycolate rods, which were produced at the beginning of the reaction, were utilized as a template for in situ Ag NPs formation and deposition in the fabrication of Ag–TiO_2 rods. The simultaneous synthesis of Ag–TiO_2 nanocomposites could be attributed to the process known as Ostwald ripening [20]. Du et al. [44] obtained a similar morphology of Ag/TiO_2 core shell nanowires using a different method. They suggested a template-induced Oswald ripening mechanism to explain the formation of the Ag/TiO_2 core-shell nanowires.

3.3. XPS

Fig. 5 shows the oxidation states of elements by XPS of the Ag–TiO_2 microrod powder. XPS spectra indicated that all samples contained Ag, Ti, O and C elements except the pure TiO_2 rods (see Fig. 5a). In Fig. 5a, the weak and unexpected peak for C1s is attributed to the residual carbon from the sample, and also to the adventitious hydrocarbon from the XPS instrument itself. The high-resolution XPS spectra of Ag 3d and Ti 2p core levels in the composite material are shown in Fig. 5b and c, respectively. A shift to lower binding energy was observed for the Ti 2p and Ag 3d of the as-synthesized Ag–TiO_2 sample when compared to the standard peaks of Ti 2p (458.5 eV) (Fig. 5c) and Ag 3d (368.2 eV) (Fig. 5b). This shift indicates the presence of Ti^{3+} produced by the heating of titanium alkoxide in ethylene glycol, and unexpected Ag–O bonds [45,45]. By comparing the high-resolution XPS spectra in Fig. 5b, it is clearly seen that the metallic silver on the surface gradually increased and becomes the dominant state after annealing. In other words, more Ag–O bonds break and more metallic silver is formed on/in the host matrix after annealing [46]. In the annealed sample (Fig. 5b), the peaks observed at 368.2 and 374.2 eV can be ascribed to Ag $3d_{3/2}$ and Ag $3d_{5/2}$ of the metallic silver, respectively. The 6.0 eV difference between the binding energy of peaks is also characteristic of metallic Ag 3d states [47,48]. In addition, no peak of oxidized silver corresponding to Ag_2O or AgO was detected. These results are in good agreement with the XRD characterization (Fig. 1). In addition, the major Ti $2p_{3/2}$ peak shifts to a higher binding energy, i.e., from 457.2 eV for the as-synthesized sample to 458.4 eV when annealed at 500 °C (Fig. 5c). A study by Wang et al. [49] reported the binding energy of the Ti2p core electron to be 457.1 eV for the as-synthesized sample, and after calcination at 450 °C, the nitrogen peak disappeared and the binding energy of Ti2p3/2 is located at 459.2 eV, corresponding to the value for anatase/ rutile. In our present sample, the binding energy of the Ti2p electrons was 458.6 eV, leaving no doubt of the existence of $Ti^{4+}O_2$ as the major titanium species [50,51].

3.4. FT-IR

To characterize the molecular nature of the material, Fourier transform infrared (FT-IR) spectra of the samples were taken. Fig. 6 shows the FT-IR spectra of the Ag–TiO_2 rods before and after annealing at 500 °C, along with those of as-synthesized pure samples. For the as-synthesized TiO_2 and Ag–TiO_2 samples (Fig. 6a and b), several absorption bands correspond to the vibrational modes of organic species such as hydroxyl, carboxilate and alkane groups are observed. In particular, the bands observed at 3370 and 1643 cm^{-1} are related to the O–H stretching mode of the hydroxyl group and the H–O–H bending mode as well as that from Ti–OH, respectively, indicating the presence of absorbed water or ethylene glycol, as reported in the literature [20,40]. The two sharp absorption bands at 2931 and 2863 cm^{-1} are attributed to the alkyl-CH_2 symmetric and asymmetric stretching [52]. At approximately 1457 cm^{-1}, a signal corresponding to the bending of –CH_2 groups appears, and the bands at 1365-1225 cm^{-1} are assigned to the scissoring of the C–H

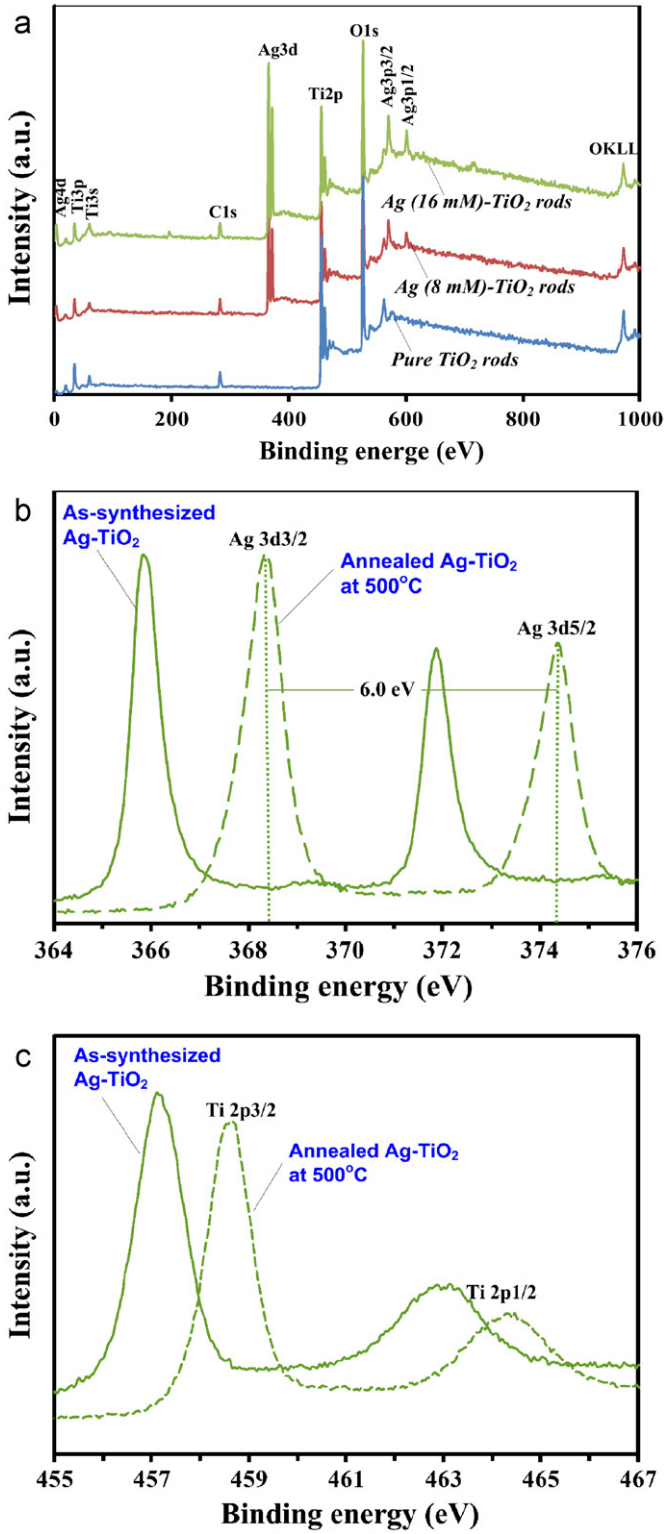

Fig. 5. XPS spectra of (a) as-synthesized TiO_2 and Ag–TiO_2 nanocomposites with different contents of $AgNO_3$, and (b,c) high-resolution XPS spectra of annealed samples at 500 °C for (b) Ag 3d and (c) Ti 2p.

bonds of the $–CH_2$ groups [40,52]. It is known that the peaks in the 1000–1200 cm^{-1} region, i.e., deformation vibrations of Ti–O–H bonds, can be observed [53,54]. The strong absorption band observed at 629 cm^{-1} not only can

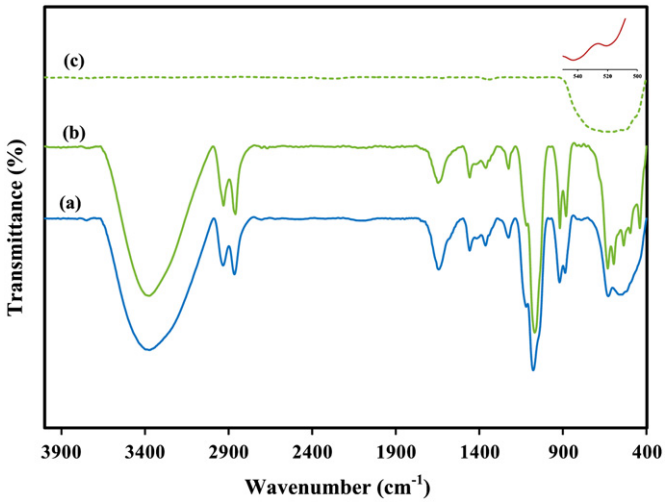

Fig. 6. FTIR spectra of (a) as-synthesized TiO_2, (b) Ag–TiO_2 microrods with 16 mM $AgNO_3$, and (c) Ag–TiO_2 microrods annealed at 500 °C.

be associated with the vibrational mode of Ti–O in the amorphous TiO_2, but also some absorption due to metal–oxygen (M–O) stretching is also seen between 400–600 cm^{-1} [42,55]. Once the amorphous structure had been transformed into the anatase phase of titania at 500 °C, the Ti–O stretching band was shifted to 543 cm^{-1}, as shown in Fig. 6c (inset). These observations were consistent with previous studies, where conventional alkoxides were used as glycolate precursors to prepare various phases of titania nanowires [20]. On the other hand, the bands attributed to the organic groups were not detected after annealing treatment, indicating its elimination in the sample.

3.5. TGA

To investigate the thermal properties of the samples during the annealing procedure, TGA was carried out at a heating rate of 10 °C min^{-1} under a nitrogen atmosphere. Fig. 7 shows the TGA curves of the Ag–TiO_2 rods before and after annealing at 500 °C, along with the as-synthesized pure samples. Analysis of the TGA thermograms of the as-synthesized pure TiO_2 rods (Fig. 7a) demonstrated an initial continuous mass loss followed by two step weight losses. The first region, the initial continuous mass loss of about 27% beginning at 25 °C and ending at 200 °C, was attributed to the desorption of physically absorbed water and ethylene glycol molecules, and the next weight loss could be ascribed to the removal of residual organic groups such as ethylene glycol units or alkyl groups chemically bonded to titanium in the microrods. The weight loss induced between 240 °C and 350 °C was about 16%. Finally, the last weight loss occurred above 510 °C, which represents approximately 11%, due to loss of glycolate ligands that are probably located in the inner part of the TiO_2 rods and phase transition [56]. However, in as-synthesized Ag–TiO_2, there are observable changes, as shown in Fig. 7b. Noticeably, the complete decomposition

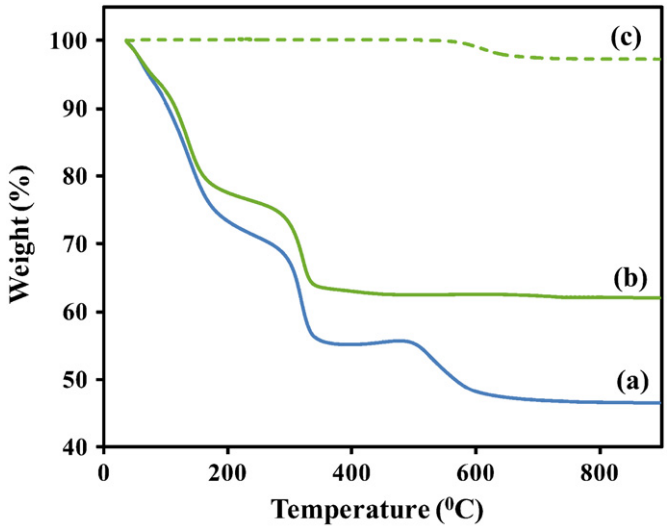

Fig. 7. TGA thermograms of (a) as-synthesized TiO_2, (b) Ag–TiO_2 microrods with 16 mM $AgNO_3$, and (c) Ag–TiO_2 microrods annealed at 500 °C.

temperature of organic groups in the pure rods (610 °C) (Fig. 7a) and composite sample (380 °C) (Fig. 7b) changed noticeably, suggesting that Ag NPs can accelerate the conversion of glycolate ligands into oxide ligands. Thermal analysis showed a slight increase in thermal stability for composite rods. The TGA curves of the Ag–TiO_2 composites annealed at 500 °C revealed only one incidence of weight loss throughout the whole measurement range, representing approximately 2% of the initial weight, indicating the elimination of practically all water and organic species by the thermal treatments before realizing the TGA analysis. These results are in good agreement with the FT-IR analysis presented earlier.

4. Conclusion

In the present study, Ag–TiO_2 rods were synthesized by a refluxing method using titanium alkoxide and silver nitrate as a starting material, ethylene glycol as the reaction medium and poly(vinylpyrrolidone) (PVP) as a capping agent under ambient conditions. As-synthesized samples were subjected to low (250 and 350 °C) and high (500 and 700 °C) annealing temperatures. Peaks of XRD analysis confirmed that supported Ag NPs partially dissolved into the host matrix under low annealing temperatures. At the same time, Ag° to Ag^{+} oxidation also occurred. However, anatase crystallization and rutile transformation of the TiO_2 matrix was promoted due to supported Ag NPs. Upon higher annealing treatment, promoting diffusion and coalescence leads to changes in the size and shape of metal particles not only in the outermost regions, but also in the random distribution and progressive growth of Ag clusters in the inner interface region of TiO_2 rods. Furthermore, the annealing process can induce chemical state (valency) and structure changes in Ag–TiO_2, and from the TGA results, the presence of Ag NPs increases the thermal stability of the TiO_2 rods.

Acknowledgments

This research was supported by a Grant from the Ministry of Education, Science and Technology of Korea through the National Research Foundation (Project no. 2011-0011807). We also thank Mr. Jong-Gyun Kang of the Center for University Research Facility of Chonbuk National University, for taking high-quality TEM images.

References

[1] J.Y. Lee, P. Peumans, The origin of enhanced optical absorption in solar cells with metal nanoparticles embedded in the active layer, Optics Express 18 (10) (2010) 10078–10087.
[2] R. Bajpai, S. Roy, P. Kumar, P. Bajpai, N. Kulshrestha, J. Rafiee, N. Koratkar, D.S. Misra, Graphene supported platinum nanoparticle counter-electrode for enhanced performance of dye-sensitized solar cells, ACS Applied Materials and Interfaces 3 (10) (2011) 3884–3889.
[3] T. Sen, S. Jana, S. Koner, A. Patra, Efficient energy transfer between confined dye and y-zeolite functionalized Au nanoparticles, Journal Of Physical Chemistry C 114 (46) (2010) 19667–19672.
[4] S.J. Guo, S.J. Dong, E.K. Wang, Raspberry-like hierarchical Au/Pt nanoparticle assembling hollow spheres with nanochannels: An advanced nanoelectrocatalyst for the oxygen reduction reaction, Journal Of Physical Chemistry C 113 (14) (2009) 5485–5492.
[5] R. Guo, R.T. Li, X.L. Li, L.Y. Zhang, X.Q. Jiang, B.R. Liu, Dual-functional alginic acid hybrid nanospheres for cell imaging and drug delivery, Small (Weinheim an der Bergstrasse, Germany) 5 (6) (2009) 709–717.
[6] H.R. Pant, D.R. Pandeya, K.T. Nam, W.I. Baek, S.T. Hong, H.Y. Kim, Photocatalytic and antibacterial properties of a TiO_2/nylon-6 electrospun nanocomposite mat containing silver nanoparticles, Journal of hazardous materials 189 (1-2) (2011) 465–471.
[7] A. Amarjargal, L.D. Tijing, C.S. Kim, One-pot synthesis of silver–titanium dioxide nanocomposites using ethylene glycol medium and their antibacterial properties, Digest Journal of Nanomaterials and Biostructures 6 (4) (2011) 1957–1965.
[8] B. Cheng, Y. Le, J. Yu, Preparation and enhanced photocatalytic activity of Ag@TiO_2 core-shell nanocomposite nanowires, Journal of Hazardous Materials 177 (1-3) (2010) 971–977.
[9] A.M. El-Kady, A.F. Ali, R.A. Rizk, M.M. Ahmed, Synthesis, characterization and microbiological response of silver doped bioactive glass nanoparticles, Ceramics International 38 (1) (2012) 177–188.
[10] M.N. An'amt, S. Radiman, N.M. Huang, M.A. Yarmo, N.P. Ariyanto, H.N. Lim, M.R. Muhamad, Sol–gel hydrothermal synthesis of bismuth–TiO_2 nanocubes for dye-sensitized solar cell, Ceramics International 36 (7) (2010) 2215–2220.
[11] J. Selva, S.E. Martinez, D. Buceta, M.J. Rodriguez-Vazquez, M.C. Blanco, M.A. Lopez-Quintela, G. Egea, Silver sub-nanoclusters electrocatalyze ethanol oxidation and provide protection against ethanol toxicity in cultured mammalian cells, Journal of the American Chemical Society 132 (20) (2010) 6947–6954.
[12] S.H. Nam, H.S. Shim, Y.S. Kim, M.A. Dar, J.G. Kim, W.B. Kim, Ag or Au nanoparticle-embedded one-dimensional composite TiO_2 nanofibers prepared via electrospinning for use in lithium-ion batteries, ACS Applied Materials and Interfaces 2 (7) (2010) 2046–2052.
[13] Y.Q. Liang, Z.D. Cui, S.L. Zhu, Y. Liu, X.J. Yang, Silver nanoparticles supported on TiO_2 nanotubes as active catalysts for ethanol oxidation, Journal Of Catalysis 278 (2) (2011) 276–287.

[14] C.L. Chen, J.G. Lee, K. Arakawa, H. Mori, In situ observations of crystalline-to-liquid and crystalline-to-gas transitions of substrate-supported Ag nanoparticles, Applied physics letters 96 (25) (2010) 253104.
[15] M. Chen, Y. Cai, Z. Yan, D.W. Goodman, On the origin of the unique properties of supported Au nanoparticles, Journal of the American Chemical Society 128 (19) (2006) 6341–6346.
[16] S.C. Tang, S.P. Zhu, H.M. Lu, X.K. Meng, Shape evolution and thermal stability of Ag nanoparticles on spherical SiO_2 substrates, Journal Of Solid State Chemistry 181 (3) (2008) 587–592.
[17] J.G. Lee, J. Lee, T. Tanaka, H. Mori, In situ HREM observation of crystalline-to-gas transition in nanometer-sized Ag particles, Physical Review Letters 96 (7) (2006) 075504-1-075504-3.
[18] A. Amarjargal, L.D. Tijing, H.R. Pant, C.-H. Park, C.S. Kim, Simultaneous synthesis of TiO_2 microrods in situ decorated with Ag nanoparticles and their bactericidal efficiency, Current Applied Physics 12 (2012) 1106–1112.
[19] Y.G. Sun, B. Gates, B. Mayers, Y.N. Xia, Crystalline silver nanowires by soft solution processing, Nano Letters 2 (2) (2002) 165–168.
[20] X.C. Jiang, Y.L. Wang, T. Herricks, Y.N. Xia, Ethylene glycol-mediated synthesis of metal oxide nanowires, Journal Of Materials Chemistry 14 (4) (2004) 695–703.
[21] L. Armelao, D. Barreca, G. Bottaro, A. Gasparotto, C. Maccato, E. Tondello, O.I. Lebedev, S. Turner, G. Van Tendeloo, C. Sada, U.L. Stangar, Rational design of Ag/TiO_2 nanosystems by a combined RF-sputtering/sol–gel approach, Chemphyschem 10 (18) (2009) 3249–3259.
[22] M. Epifani, C. Giannini, L. Tapfer, L. Vasanelli, Sol–gel synthesis and characterization of Ag and Au nanoparticles in SiO_2, TiO_2, and ZrO_2 thin films, Journal of the American Ceramic Society 83 (10) (2000) 2385–2393.
[23] A. Henglein, Colloidal silver nanoparticles: Photochemical preparation and interaction with O-2, CCl4, and some metal ions, Chemistry of Materials 10 (1) (1998) 444–450.
[24] G.V. Krylova, Y.I. Gnatyuk, N.P. Smirnova, A.M. Eremenko, V.M. Gun'ko, Ag nanoparticles deposited onto silica, titania, and zirconia mesoporous films synthesized by sol–gel template method, Journal of Sol–Gel Science Technology 50 (2) (2009) 216–228.
[25] J.M. Wu, C.J. Chen, Dielectric-properties of (Ba,Nb) doped TiO_2 ceramics—migration mechanism and roles of (Ba,Nb)., Journal Of Materials Science 23 (11) (1988) 4157–4164.
[26] L. Vitos, A.V. Ruban, H.L. Skriver, J. Kollar, The surface energy of metals, Surface Science 411 (1-2) (1998) 186–202.
[27] D.A. Chen, M.C. Bartelt, S.M. Seutter, K.F. McCarty, Small, uniform, and thermally stable silver particles on $TiO_2(1\,1\,0)$-(1×1), Surface Science 464 (1) (2000) L708–L714.
[28] C. Suwanchawalit, S. Wongnawa, P. Sriprang, P. Meanha, Enhancement of the photocatalytic performance of Ag-modified TiO_2 photocatalyst under visible light, Ceramics International, http://dx.doi.org/10.1016/j.ceramint.2012.03.027., in press.
[29] B.A. Akgun, C. Durucan, N.P. Mellott, Effect of silver incorporation on crystallization and microstructural properties of sol–gel derived titania thin films on glass, Journal of Sol–Gel Science and Technology 58 (1) (2011) 277–289.
[30] H.E. Chao, Y.U. Yun, H.U. Xingfang, A. Larbot, Effect of silver doping on the phase transformation and grain growth of sol–gel titania powder, Journal Of The European Ceramic Society 23 (9) (2003) 1457–1464.
[31] A. Ahmad, J. Thiel, S.I. Shah, Structural effects of niobium and silver doping on titanium dioxide nanoparticles, Journal of Physics: Conference Series 61 (2007) 11–15.
[32] G. Oliveri, G. Ramis, G. Busca, V.S. Escribano, Thermal-stability of vanadia–titania catalysts, Journal Of Materials Chemistry 3 (12) (1993) 1239–1249.
[33] T.L. Thompson, J.T. Yates, TiO_2-based photocatalysis: surface defects, oxygen and charge transfer, Topics in Catalysis 35 (3–4) (2005) 197–210.
[34] W.D. Kingery, H.K. Bowen, D.R. Uhlmann, Introduction to Ceramics, 2nd ed., John Wiley and Sons, New York, 1976, pp. 448–459.
[35] J. Okumu, C. Dahmen, A.N. Sprafke, M. Luysberg, G. von Plessen, M. Wuttig, Photochromic silver nanoparticles fabricated by sputter deposition, Journal of Applied Physics 97 (9) (2005) 094305-1-094305-6.
[36] J. Okumu, D. Kohl, A. Sprafke, G. von Plessen, M. Wuttig, Formation mechanism of noble metal nanoparticles in reactively sputtered TiO_2 films, Journal of applied physics 108 (6) (2010) 063529-1-063529-5.
[37] R.C. Adochite, D. Munteanu, M. Torrell, L. Cunha, E. Alves, N.P. Barradas, A. Cavaleiro, J.P. Riviere, E. Le Bourhis, D. Eyidi, F. Vaz, The influence of annealing treatments on the properties of $Ag:TiO_2$ nanocomposite films prepared by magnetron sputtering, Applied Surface Science 258 (8) (2012) 4028–4034.
[38] J. Garcia-Serrano, E. Gomez-Hernandez, M. Ocampo-Fernandez, U. Pal, Effect of Ag doping on the crystallization and phase transition of TiO_2 nanoparticles, Current Applied Physics 9 (5) (2009) 1097–1105.
[39] S. Priya, J. Robichaud, M.C. Methot, S. Balaji, J.M. Ehrman, B.L. Su, Y. Djaoued, Transformation of microporous titanium glycolate nanorods into mesoporous anatase titania nanorods by hot water treatment, Journal of Materials Science 44 (24) (2009) 6470–6483.
[40] Q. Li, B. Liu, Y. Li, R. Liu, X. Li, D. Li, S. Yu, D. Liu, P. Wang, B. Li, B. Zou, T. Cui, G. Zou, Ethylene glycol-mediated synthesis of nanoporous anatase TiO_2 rods and rutile TiO_2 self-assembly chrysanthemums, Journals of Alloys and Compounds 471 (1–2) (2009) 477–480.
[41] D. Kim, S. Jeong, J. Moon, Synthesis of silver nanoparticles using the polyol process and the influence of precursor injection, Nanotechnology 17 (16) (2006) 4019–4024.
[42] S. Duhan, S. Devi, M. Srivastava, Characterization of nanocrystalline Ag/SiO_2 nanocomposites and synthesis by wet chemical method, Indian Journal Of Pure & Applied Physics 48 (4) (2010) 271–275.
[43] M. Asoro, J. Damiano, P.J. Ferreira, Size effects on the melting temperature of silver nanoparticles: in-situ TEM observations, Microscopy and Microanalysis 15 (S2) (2009) 706–707.
[44] J.M. Du, J.L. Zhang, Z.M. Liu, B.X. Han, T. Jiang, Y. Huang, Controlled synthesis of Ag/TiO_2 core-shell nanowires with smooth and bristled surfaces via a one-step solution route, Langmuir 22 (3) (2006) 1307–1312.
[45] M.C. Biesinger, L.W.M. Lau, A.R. Gerson, R.S.C. Smart, Resolving surface chemical states in XPS analysis of first row transition metals, oxides and hydroxides: Sc, Ti, V, Cu and Zn, Applied Surface Science 257 (3) (2010) 887–898.
[46] P.W. Wang, Y.F. Jiang, J.C. Hsu, Y.Y. Chen, Y.H. Lin, H.L. Chen, Thermal effect on structure of silver in ion-exchanged soda-lime glasses and aluminum-doped zinc oxide films, Advances in Material Science and Engineering (2011) 1–6.
[47] H.J. Zhang, G.H. Chen, Potent antibacterial activities of Ag/TiO_2 nanocomposite powders synthesized by a one-pot sol–gel method, Environmental Science & Technology 43 (8) (2009) 2905–2910.
[48] Y. Liu, J.C. Hu, J.L. Li, Synthesis and photoactivity of the highly efficient Ag species/TiO_2 nanoflakes photocatalysts, Journal of Alloys and Compounds 509 (16) (2011) 5152–5158.
[49] Y.Q. Wang, S.G. Chen, X.H. Tang, O. Palchik, A. Zaban, Y. Koltypin, A. Gedanken, Mesoporous titanium dioxide: sonochemical synthesis and application in dye-sensitized solar cells, Journal of Materials Chemistry 11 (2) (2001) 521–526.
[50] Y.K. Lai, Y.C. Chen, H.F. Zhuang, C.J. Lin, A facile method for synthesis of Ag/TiO_2 nanostructures, Materials Letters 62 (21-22) (2008) 3688–3690.
[51] L.X. Mai, D.W. Wang, S. Zhang, Y.J. Xie, C.M. Huang, Z.G. Zhang, Synthesis and bactericidal ability of Ag/TiO_2 composite

films deposited on titanium plate, Applied Surface Science 257 (3) (2010) 974–978.
[52] M.D. Wei, H.S. Zhou, Y. Konishi, M. Ichihara, H. Sugiha, H. Arakawa, Synthesis of tubular titanate via a self-assembly and self-removal process, Inorganic Chemistry 45 (14) (2006) 5684–5690.
[53] P. Jackson, G.D. Parfitt, Infra-red study of surface properties of rutile—water and surface hydroxyl species, Transactions of the Faraday Society 67 (584) (1971) 2469.
[54] N. K., Infrared and Raman Spectra of Inorganic and Coordination Compounds, fourth ed., Wiley, New York, 1986, p. 230.
[55] T. Bezrodna, G. Puchkovska, V. Shymanovska, J. Baran, H. Ratajczak, IR-analysis of H-bonded H_2O on the pure TiO_2 surface, Journal of Molecular Structure 700 (1-3) (2004) 175–181.
[56] V.G. Pol, Y. Langzam, A. Zaban, Application of microwave superheating for the synthesis of TiO_2 rods, Langmuir 23 (22) (2007) 11211–11216.